NASA Contractor Report 172353

ICASE REPORT NO. 84-15

ICASE

A NUMERICAL STUDY OF THE TWO- AND THREE-DIMENSIONAL UNSTEADY NAVIER-STOKES EQUATIONS IN VELOCITY-VORTICITY VARIABLES USING COMPACT DIFFERENCE SCHEMES

Thomas B. Gatski

and

Chester E. Grosch

Contract No. NAS1-17070

May 1984

INSTITUTE FOR COMPUTER APPLICATIONS IN SCIENCE AND ENGINEERING
NASA Langley Research Center, Hampton, Virginia 23665

Operated by the Universities Space Research Association

NASA
National Aeronautics and
Space Administration

Langley Research Center
Hampton, Virginia 23665

A NUMERICAL STUDY OF THE TWO- AND THREE-DIMENSIONAL UNSTEADY NAVIER-STOKES EQUATIONS IN VELOCITY-VORTICITY VARIABLES USING COMPACT DIFFERENCE SCHEMES

Thomas B. Gatski
NASA Langley Research Center, Hampton, VA 23665

Chester E. Grosch
Institute for Computer Applications in Science and Engineering
and
Old Dominion University, Norfolk, VA 23508

Abstract

A compact finite-difference approximation to the unsteady Navier-Stokes equations in velocity-vorticity variables is used to numerically simulate a number of flows. These include two-dimensional laminar flow of a vortex evolving over a flat plate with an embedded cavity, the unsteady flow over an elliptic cylinder, and aspects of the transient dynamics of the flow over a rearward facing step. The methodology required to extend the two-dimensional formulation to three-dimensions is presented.

Research for the second author supported by the National Aeronautics and Space Administration under NASA Contract No. NAS1-17070 while he was in residence at ICASE, NASA Langley Research Center, Hampton, VA 23665.

Introduction

We present a solution method for the unsteady Navier-Stokes equations expressed in velocity-vorticity variables. Although this formulation is somewhat unusual, incompressible flow fields can be regarded as a realization of vorticity dynamics and as being driven by the production of vorticity at the boundaries.

Most algorithms for the incompressible Navier-Stokes equations are couched in either stream function, vorticity variables in two-dimensions, or in so-called primitive variables of pressure and velocity in either two- or three-dimensions. When the stream function, vorticity formulation is used, accuracy can be degraded in differencing the stream function to obtain boundary values for the vorticity. Difficulties can arise, when using the primitive variable approach, in calculating the pressure boundary conditions and in maintaining the incompressibility condition.

The formulation of the Navier-Stokes equations in terms of velocity and vorticity is an alternate approach. Dennis, Ingram, and Cook (1979) and Fasel (1980) have also used this formulation as the basis of numerical calculations. Dennis et al treated the steady-state problem in three dimensions and Fasel treated the time-dependent problem in two dimensions. In both of these studies, Poisson equations for the velocity components were derived from the kinematic definition of vorticity and used in the solution algorithm. In the numerical method developed by Gatski, Grosch, and Rose (1982) (GGR, hereafter) and used here, the kinematic definition of vorticity is used directly, along with the incompressibility condition of a divergence free-velocity field. These equations, coupled with the transport equation for the vorticity, form the basis of the algorithm.

The finite-difference schemes used are members of a class of compact finite-difference schemes described by Keller (1974), Rose (1981), Philips and Rose (1982). They have been used by Wornom (1977), GGR, and Malik, Chuang, and Hussaini (1982). These compact schemes appear to have some advantages over more conventional central and upwind-difference schemes. Some of these advantages are that they are second-order accurate, independent of the value of the local cell Reynolds number, and require only values of the dependent variables in, and on, the boundaries of a single cell, thus easing the calculation of boundary conditions and the use of stretched grids.

In addition to the formulation and test of the method (GGR), the algorithm has been applied to the laminar flow over an embedded cavity (Gatski and Grosch, 1984) and the unsteady forced flow of a shear layer (McInville, Gatski, and Hassan, 1984). Results presented here include the interaction of a Stuart vortex (Gatski, 1983) with an embedded cavity in laminar boundary layer flow, the unsteady flow past an elliptic cylinder, and the flow past a rearward facing step in a channel.

Solution Method

The basic development and formalism for the two-dimensional solution method are described in GGR. In the present work, the boundary specification has been altered in the vortex over an embedded cavity example to account for the incoming vortical motion, and in the elliptic cylinder example, the solution method is applied to the flow in a non-Cartesian coordinate system.

For completeness, it is appropriate to give a brief outline of the method used in the solution of the two-dimensional problem. The governing

defferential equations for the solution set are those for an incompressible laminar flow,

$$u^{i}_{,i} = 0 \tag{1}$$

$$\zeta^{i} = \varepsilon^{ijk} u_{k,j} \tag{2}$$

$$\zeta^{i}_{t} + u^{j}\zeta^{i}_{,j} - \zeta^{j}u^{i}_{,j} = Re^{-1} g^{jk}\zeta^{i}_{,jk} \tag{3}$$

where in Cartesian coordinates for example

$$x^{i} = (x,y,z);\ u^{i} = (u,v,w);\ \zeta^{i} = (\zeta^{1},\zeta^{2},\zeta^{3}), \tag{4a,b,c}$$

Re is a suitably defined Reynolds number based on the characteristic velocity and length scales of the flow and the kinematic viscosity of the fluid. Equations (1) through (3) are written in generalized tensor notation, with g^{jk} the metric tensor, to expedite the coordinate transformation discussion to be presented later. In the following presentation of the numerical method, the discussion is limited to the two-dimensional Cartesian case and the x and y component velocities given by u and v, respectively, and the nonzero vorticity component given by $\zeta = \zeta^{3}$. The finite-difference approximations to Equations (1) through (3) are given by GGR

$$\delta_{x} u^{n}_{\bullet} + \delta_{y} v^{n}_{\bullet} = 0; \quad \delta_{x} v^{n}_{\bullet} - \delta_{y} u^{n}_{\bullet} = \zeta^{n-1/2}_{\bullet} \tag{5a,b}$$

with auxiliary conditions

$$(\mu_x - \mu_y)u^n_{\cdot\cdot} = 0; \quad (\mu_x - \mu_y)v^n_{\cdot\cdot} = 0 \tag{6a,b}$$

and

$$(\delta_t + (\mu_x u^n_{\cdot\cdot})\delta_x + (\mu_y v^n_{\cdot\cdot})\delta_y)\zeta^n_{\cdot\cdot} = Re^{-1}(\delta_x \phi^n_{\cdot\cdot} + \delta_y \psi^n_{\cdot\cdot}) \tag{7a}$$

$$\delta_x \zeta^n_{\cdot\cdot} = (\mu_x - 1/2\ \Delta x q_x \delta_x)\phi^n_{\cdot\cdot}; \quad \delta_y \zeta^n_{\cdot\cdot} = (\mu_y - 1/2\ \Delta y q_y \delta_y)\psi^n_{\cdot\cdot} \tag{7b,c}$$

with auxiliary conditions

$$\mu_t \zeta^n_{\cdot\cdot} = \mu_x \zeta^n_{\cdot\cdot} = \mu_y \zeta^n_{\cdot\cdot} \tag{8}$$

The dot subscript notations used in Equations (5) through (8) implies average and difference operations about cell centers, and the variables q_x and q_y are functions of the respective cell Reynolds numbers and are given by

$$q_x = \coth \theta_x - \theta_x^{-1}; \quad q_y = \coth \theta_y - \theta_y^{-1} \tag{9a,b}$$

where

$$\theta_x = u_{\cdot\cdot}\Delta x Re/2; \quad \theta_y = v_{\cdot\cdot}\Delta y Re/2 \tag{10a,b}$$

The solution method consists of an alternation between a velocity solver, described in GGR, for the velocity equations, Equations (5) and (6); and a vorticity solver, also described in GGR, for the vorticity equations, Equations (7) and (8). This methodology along with the appropriate time-dependent inflow boundary conditions described later constitute the technique used in solving the evolving vortex flow example.

The solution method just described can also be directly applied to the solution of the unsteady flow over an elliptic cylinder by first transforming

the coordinate basis set from Cartesian to elliptic cylindrical. Consider the transformation

$$x = (a^2 - b^2)^{1/2} \cosh \xi \cos \eta; \quad y = (a^2 - b^2)^{1/2} \sinh \xi \sin \eta \qquad (11a,b)$$

where a and b are the semi-major and semi-minor axes of the ellipse, respectively; and lines of constant ξ and η are confocal ellipses and hyperbolas, respectively. This system is particularly advantageous since the non-zero elements of the metric tensor are equal, that is

$$g^{jk} = \begin{pmatrix} (a^2 - b^2)(\sinh^2 \xi + \sin^2 \eta) & 0 & 0 \\ 0 & (a^2 - b^2)(\sinh^2 \xi + \sin^2 \eta) & 0 \\ 0 & 0 & 0 \end{pmatrix} \qquad (12)$$

Thus the vorticity transport equation, expressed in ξ, η variables as well as the respective physical component velocities, is of the same form as the corresponding Cartesian vorticity equation. This then allows for the direct application of the difference equations, given in Equations (5) through (8) for the Cartesian system, to the differential equations governing the elliptic cylinder problem.

Stream function and pressure values can be calculated from the computed velocity and vorticity variables. The stream function values are obtained directly from the velocity field by a simple integration of the velocity along the edge of each cell. This then determines the stream function values at the corners of each computational cell. The pressure field is more complex in that the pressure values are determined from the x and y momentum

equations and as such must be defined at the midpoint of the cell edges to be consistent with the velocity and voricity variable locations. A consistent means, therefore, of obtaining the pressure field is to use a solution procedure which is analogous to the one used in the velocity solver. This can be done by first writting the u and v momentum equations, or their non-Cartesian analogs in the case of the elliptic cylinder, as

$$\partial p/\partial x = -(u_t + uu_x + vu_y + Re^{-1}\zeta_y) = L_x(u,\zeta) \qquad (13a)$$

$$\partial p/\partial y = -(v_t + uv_x + vv_y - Re^{-1}\zeta_x) = L_y(v,\zeta) \quad , \qquad (13b)$$

where all the terms on the right side of Equations (13a) and (13b) are known at each time step. Next, recombine these equations into the more adaptable form

$$\partial p/\partial x + \partial p/\partial y = L_x + L_y \; ; \; \partial p/\partial x - \partial p/\partial y = L_x - L_y \qquad (14a,b)$$

Recall that the pressure variables are defined along the edges of each computational cell. If the pressure variables defined along the vertical edges (lines of constant x) are designated P_V and those defined along the horizontal edges (lines of constant y) are designated P_H, then the following discretization, of Equation (14) holds

$$\delta_x P_V + \delta_y P_H = \Omega(L_x + L_y); \; \delta_x P_V - \delta_y P_H = \Omega(L_x - L_y), \qquad (15a,b)$$

along with the auxiliary conditions

$$\mu_x P_V - \mu_y P_H = 0 \tag{15c}$$

Since Equation (15) is an analog of Equations (5) and (6), the solver which was applied to the discretized velocity equations can be applied directly to the above discretized pressure equations.

The results presented in the next section and from those presented in previous studies (Gatski and Grosch, 1984; McInville, Gatski, and Hassan, 1984) show that the algorithm is adaptable to a rather wide class of two-dimensional unsteady flows. It is desirable to extend this methodology to three-dimensional unsteady flows. As was the case in the two-dimensional problem, the differential equation set, Equations (1) through (3), are used directly in the three-dimensional problem. Equations (1) and (2), which once again constitute the velocity solver, are discretized using box-variables to represent the velocities and assigning the vorticity values to the center of each computational box. Such a formulation produces an over-determined system; however, Fix and Rose (1984) have shown that such a finite-difference approximation yields a least squares solution which is second order accurate. This velocity field is then used to calculate vorticity boundary conditions through second order accurate difference approximations at the boundaries. Before the vorticity transport equations can be brought into the solution sequence a modification to the form of the equations needs to be made. This is necessary because the three-dimensional vorticity transport equations contain a vortex stretching term which negates the direct use of the finite-difference basis set which was used in the two-dimensional transport equation. Recall, however, that as the vorticity equations are solved over a time step Δt, the form of the equations allows for the introduction of an

integrating factor (Rose, private communication) which transforms the vorticity transport equations into simple advection-diffusion equations. This system can then be solved for the three component vorticities in a completely analogous manner to the simple two-dimensional equation.

This completes the outline of the methodology that can be used in the solution of a class of two- and three-dimensional unsteady flows. In the next section, the application of this solution technique to a few relevant flow problems is presented.

Computational Results

In this section some results from the numerical solution of three two-dimensional unsteady flows will be presented. The two-dimensional flows include the evolution of a vortical structure over an embedded cavity, the unsteady flow over an elliptic cylinder, and some aspects of the flow over a rearward facing step in a channel.

Consider first the evolution of a vortical structure over an embedded cavity. Such a flow is of interest since it serves as a qualitative model of a large scale vortical structure, omnipresent in wall bounded turbulent shear flows, evolving over an isolated surface roughness represented by an embedded cavity. The reference flow field, in the absence of the perturbing vortical structure, is a laminar boundary layer flow over an embedded cavity. This flow has been extensively studied numerically in Gatski and Grosch (1984) where such flow field characteristics as wall shear stress and pressure distributions as well as the usual vorticity and stream function contours have been presented. In the present study, a Stuart vortex is introduced at the

inflow boundary in a consistent mathematical manner through the method of matched asymptotic expansions (Gatski, 1983); and flow characteristics similar to those obtained in the unperturbed case are obtained at different times in the evolution of the vortex over the cavity. Figure 1 shows the vorticity, stream function and pressure contours of the flow when the vortex has evolved to a point directly above the embedded cavity. Here, the cavity is square and has a depth of one-half of the inflow boundary layer thickness. The vorticity contours are shown in Figure 1a. The figure shows the main vortical motion above the cavity as well as a remnant of an induced vortical region downstream of the main motion. This induced structure was originally formed by the interaction of the Stuart vortex with the bounding wall; however, as the main vortex evolved to the point shown in the figure, the strength of this induced vortex was weakened by the embedded cavity. Figure 1b shows an enlarged view of the motion in the cavity, as represented by the stream function contours, when the vortex is in the position shown in Figure 1a. It is, of course, realized that any interpretation of the unsteady motion of the fluid in terms of the stream function must be done with caution; however, to be consistent with the previous work done on this same flow geometry (Gatski and Grosch, 1984) but without the vortex, the stream function contours are qualitatively informative. In the unperturbed flow, the cavity vortex was bounded by the cavity walls and by a slightly convex zero streamline, which indicated a local acceleration of the flow in the vicinity of the cavity. The results shown in Figure 1b indicate that the vortex in the boundary layer causes the cavity vortex to lift out of the cavity. This type of vortex action is a significant factor in the alteration of the drag characteristics of turbulent flow over surface roughnesses. In Figure 1c is shown the pressure contours in the

boundary layer. The figure clearly shows the low pressure regions associated with the area beneath the vortices and the high pressure region associated with the flow which is directed toward the wall by the main vortex. This pictoral representation of the perturbed cavity flow is intended to serve as an indicator of the rather complex dynamics which takes place in this type of flow field. The additional computational results which have been obtained from this study have allowed for the accurate calculation of such quantities as wall shear stress and wall pressure distributions which are used to quantify the drag characteristics of such flows.

A second example is the impulsive start of the flow over an elliptic cylinder. This is an example of the unsteady separation of an external flow. The impulsive start of a circular cylinder is, of course, a classic problem, but there seems to be no numerical work for the elliptic cylinder. We are beginning a systematic program of such calculations, in the course of which we intend to vary the Reynolds number, slenderness of the ellipse, and angle of attack.

Some preliminary results are shown in Figure 2 at a time shortly after the beginning of separation. Here the Reynolds number, with the length scale based on the semi-major axis,is 100, the ratio of major to minor axis is 2, and the angle of attack is zero. The computational domain is $0 < \eta \leq 2\pi$, $0.5493 \leq \xi \leq 4.2493$; the outer boundary is approximately that of a circle with radius $\simeq$ 22a. There are 120 cells in the η direction with a width of $\pi/60$, and 50 cells in the ξ direction. Variable cell heights, ranging from 0.01 to 1.0, are used in the ξ direction in order that the boundary layer can be resolved. The velocity and vorticity are specified on the forward portion $(\pi/2 \leq \eta \leq 3\pi/2)$ of the outer boundary. Outflow boundary conditions

are applied to the remainder of the outer boundary. The initial condition is that the flow is that given by the potential solution.

The vorticity distribution, as shown in Figure 2a, is determined by a balance between diffusion and advection. Vorticity is produced at the boundary and is diffused away. Simultaneously it is advected towards the rear of the ellipse. This leads to the appearance of a rather thin region of non-zero vorticity on the forward part of the ellipse and the long "tails" of vorticity streaming from the body. This has been observed in both start-up and steady flow past circular cylinders and is discussed by Batchelor (1967). In contrast, the stream function results given in Figure 2b indicate that the overall velocity field is only slightly different from that of the potential flow. A thin region of separation is also apparent in Figure 2, but at this early time a viscous wake has not yet formed. Finally, it can be seen from the results shown in this figure that the flow field is nearly, but not quite symmetric about $\eta = 0, \pi$. Symmetry conditions are not imposed on the solution, but the velocity and vorticity are required to be periodic in η and they are symmetric at $t = 0$. This asymmetry is due to small perturbations which are caused by the sweep direction bias in the solvers.

Another example of practical relevance is the flow in a channel with a backward facing step. This is a simple prototype of a separating internal flow. Figures 3a and 3b show the steady-state distribution of the stream function and vorticity contours for this flow at $Re = 300$. The Reynolds number, Re, length scale is the height of the inflow channel and the velocity scale is the maximum speed at inflow. The inflow boundary conditions are a parabolic velocity profile and a linear distribution for the vorticity. The outflow boundary condition assumed a zero cross-stream component of velocity,

v, and a simple advective flux of vorticity across the outflow. The geometry of Figure 3 has been considerably distorted in order to display the results clearly. The height of the inflow channel and of the step is one unit. The length of the inflow region, upstream of the step, is four units, and the length of the channel downstream of the step is 30 units. The computational cells are of constant height, 0.04, in the cross-channel direction so that there are, across the channel, 25 cells in the entrance region and 50 cells downstream of the step. The importance of having good resolution near the step and the reattachment point, combined with the great length (34 units) of the computational domain required that variable grids be used along the channel. A total of 130 cells were used with the cell width varying from 0.01 to 0.5.

As can be seen from the results of Figure 3, there is, at this Reynolds number, virtually no upstream effect of the step. It was found that the deviation from a parabolic velocity and linear vorticity profile was less than 10^{-3} one unit upstream of the step. Thus, an entrance region four units long is more than adequate. In contrast, a computational domain which is 30 units long downstream of the step is, at this Re, only just adequate. Originally, the region downstream of the step was taken to be 20 units long. It was found that this was too short. The velocity and vorticity profiles in the outflow region were distorted and not symmetric about the centerline of the channel. Considerable numerical experimentation led to the conclusion that this was due to the channel being too short; thus the computational domain was lengthened by 10 units.

The present results show that the flow over the step generates a rather weak corner vortex, at least at this low Re. The speed of the reverse flow

in this vortex is less than 10 percent of the maximum inflow speed. It appears that there is a diffusive dominance in the cross-channel direction and an advective dominance along the channel. One result of this is that the effect of the step persists, in the lower half of the channel for very large distances downstream. In the upper half of the channel, there is a region of decelerating flow downstream of the step and over the recirculation zone. This deceleration, combined with the frictional drag of the upper wall gives a region of near separation on the upper wall. We have found that at slightly higher Re, a zone of laminar separation and reattachment forms on the upper wall. Beyond the separation or near separation zone, the readjustment of the flow is due to a cross-channel diffusion of streamwise momentum. A long length of channel is required for this process to be completed.

As has been shown, this flow field is stable, but that does not prevent the formation of stable, that is decaying, shear waves. Any impulsive change in the flow will excite these transient waves. An example is shown in Figure 4. The flow field at $Re = 300$ was perturbed by decreasing the viscosity so that the Reynolds number was instantaneously changed from 300 to 500. Contours of the instantaneous values of stream function and vorticity are given in Figures 4a and 4b, respectively. These results are at approximately 20 time units after the viscosity was changed and show large amplitude shear waves in the channel. Note that these waves are downstream of the separation zone behind the step; which is, in fact, where they were formed. A comparison of Figures 4a and 4b show that the vorticity field is a more sensitive indicator than the stream function. The waves near the downstream boundary are quite visible in the vorticity contours, while they are nearly absent in the same region of the plot of the instantaneous streamlines. There is a

maximum of approximately 0.73 in the stream function downstream of the step and near the upper boundary, which is considerably above 2/3, the maximum value of the stream function at inflow and outflow. Finally, there is a separation region on the upper wall, as shown by the region of negative vorticity, which is assocsiated with this stream function maximum.

Finally, the three-dimensional formulation which was described in the previous section is presently being applied to the study of the time-dependent behavior of a single Taylor-Green vortex. As is known such a vortex is described by a simple diffusion equation for each vorticity component and serves as an excellent check on the diffusive characteristics of the numerical algorithm in three dimensions. In addition, since the structure of the Taylor-Green vortex is known analytically, this model problem is also a useful means of checking the accuracy of the overall solution method. Work on the Taylor-Green problem is in its early stages and will be presented elsewhere.

Concluding Remarks

The results presented in this study have shown that the compact vorticity-velocity difference formulation used is readily adaptable to a rather large class of unsteady fluid flow problems. In addition, the results from this and previous studies have shown that the computed results are of sufficient accuracy to describe detailed dynamic features of these flows. Future efforts in this area include further development of the three-dimensional formulation and methodology, and the adaptation of this compact difference formulation to the new generation of concurrent processors with the goal of extending the range of real flows that can be treated in the present context.

References

1. Batchelor, G. K.: An Introduction to Fluid Dynamics. Cambridge University Press, Cambridge, 1967.

2. Dennis, S. C. R.; Ingham, D. B.; and Cook, R. N.: Finite-Difference Methods for Calculating Steady Incompressible Flows in Three Dimensions. J. Comp. Phys., Vol. 33, (1978), pp. 325-339.

3. Fasel, H. F.: Numerical Solution of the Complete Navier-Stokes Equations for the Simulation of Unsteady Flows. Lecture Notes in Mathematics, No. 771, Springer-Verlag, New York/Berlin, (1980), pp. 177-195.

4. Fix, G. J.; and Rose, M. E.: A Comparative Study of Finite Element and Finite-Difference Methods for Cauchy-Riemann Type Equations. SIAM J. Numerical Analysis, (1984), to appear.

5. Gatski, T. B.; Grosch, C. E.; and Rose, M. E.: A Numerical Study of the Two-Dimensional Navier-Stokes Equations in Vorticity-Velocity Variables. J. Comp. Phys., Vol. 48, No. 1, (1982), pp. 1-22.

6. Gatski, T. B.: The Disturbance Flow Field Produced by an Evolving Vortex. NASA TP 2245, December 1983.

7. Gatski, T. B.; and Grosch, C. E.: Embedded Cavity Drag in Steady and Unsteady Flows. AIAA 22nd Aerospace Sciences Meeting, Paper No. 84-0436, January 9-12, 1984, Reno, Nevada.

8. Keller,H. K.: Accurate Difference Methods for Nonlinear Two-Point Boundary Value Problems. SIAM J. Numerical Analysis, Vol. 11, No. 2, (1974), pp. 305-320.

9. Malik, M. R.; Chuang, S.; and Hussaini, M. Y.: Accurate Numerical Solution of Compressible, Linear Stability Equations. Journal of Applied Mathematics and Physics (ZAMP), Vol. 33, No. 2, (1982), pp. 189-201.

10. McInville, R. M.; Gatski, T. B.; and Hassan,, H. A.: Embedded Shear Layer Computations for Increased Drag Reduction. AIAA 22nd Aerospace Sciences Meeting, Paper No. 84-0349, January 9-12, 1984, Reno, Nevada.

11. Philips, R. B.; and Rose, M. E.: Compact Finite-Difference Schemes for Mixed Initial-Boundary Value Problems. SIAM J. Numerical Analysis, Vol. 19, No. 4, (1982), pp. 698-720.

12. Rose, M. E.: A "Unified" Numerical Treatment of the Wave Equation and the Cauchy-Riemann Equations. SIAM J. Numerical Analysis, Vol. 18,No. 2, (1981), pp. 372-376.

13. Wornom, S. F.: Critical Study of Higher Order Numerical Methods for Solving the Boundary-Layer Equations. NASA TP 1302, November 1978.

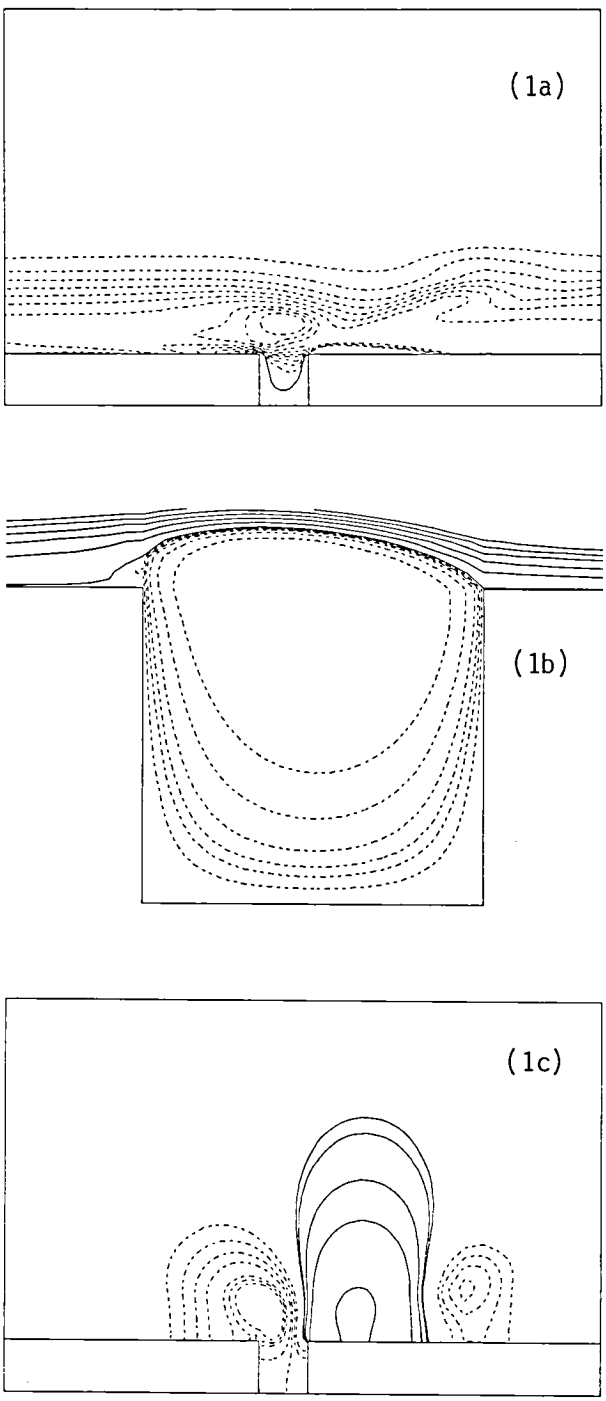

Figure 1: (1a) Vorticity contours in boundary layer (contour levels -1.8 to 0.0); (1b) Stream function contours in embedded cavity (contour levels -0.002 to 0.005); (1c) Pressure contours in boundary layer (contour levels -0.017 to 0.10).

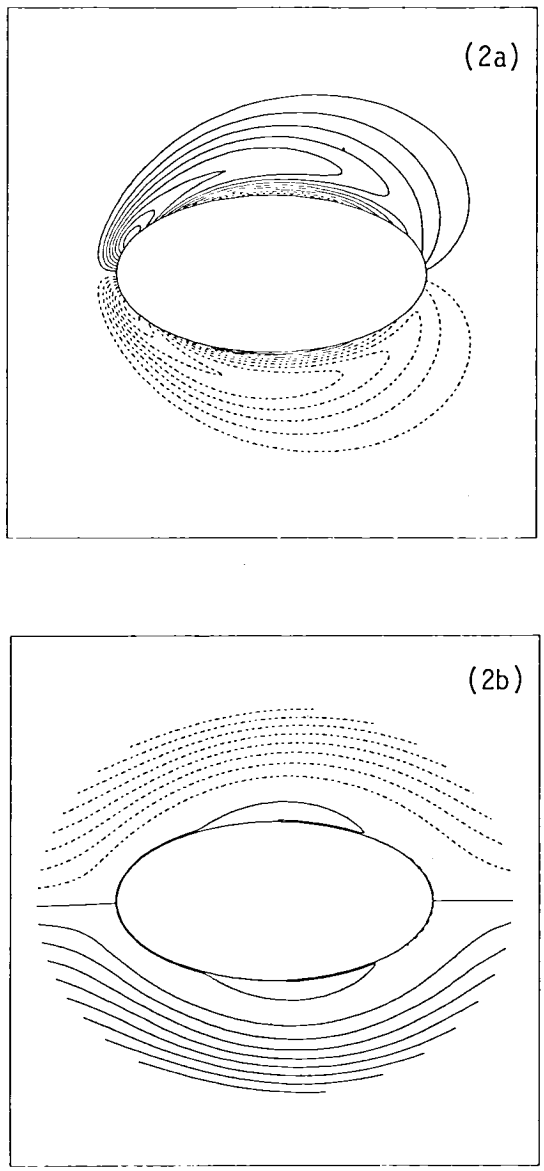

Figure 2: (2a) Vorticity contours in near field of elliptic cylinder (contour levels -6.40 to 6.40); (2b) Stream function contours in near field of elliptic cylinder (contour levels -0.56 to 0.56).

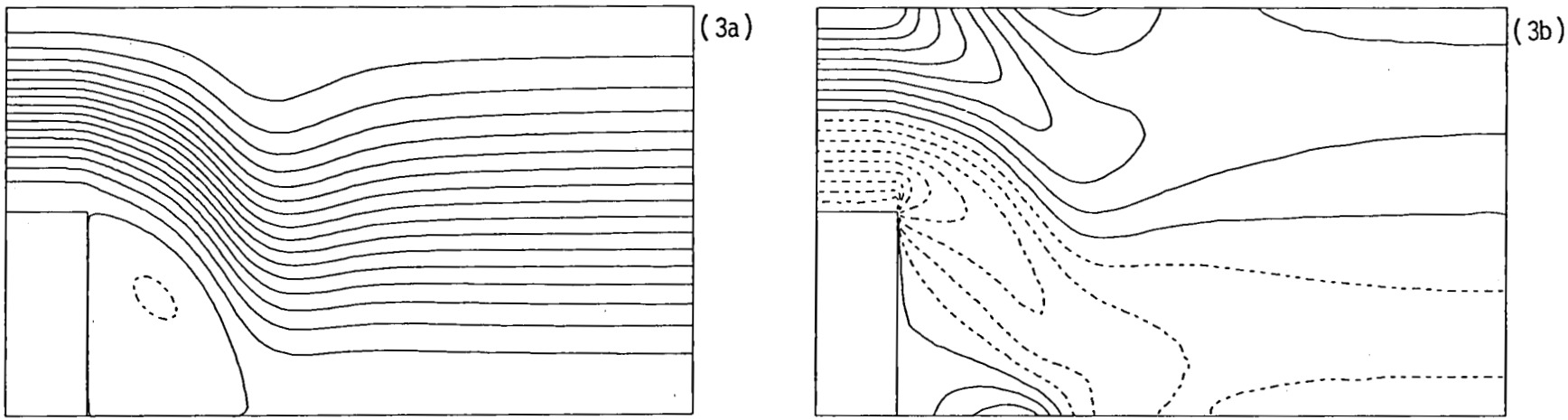

Figure 3: Channel flow with rearward facing step at Re = 300: (3a) Stream function contours (contour levels 0.0 to 2/3); (3b) Vorticity contours (contour levels -3.60 to 3.60).

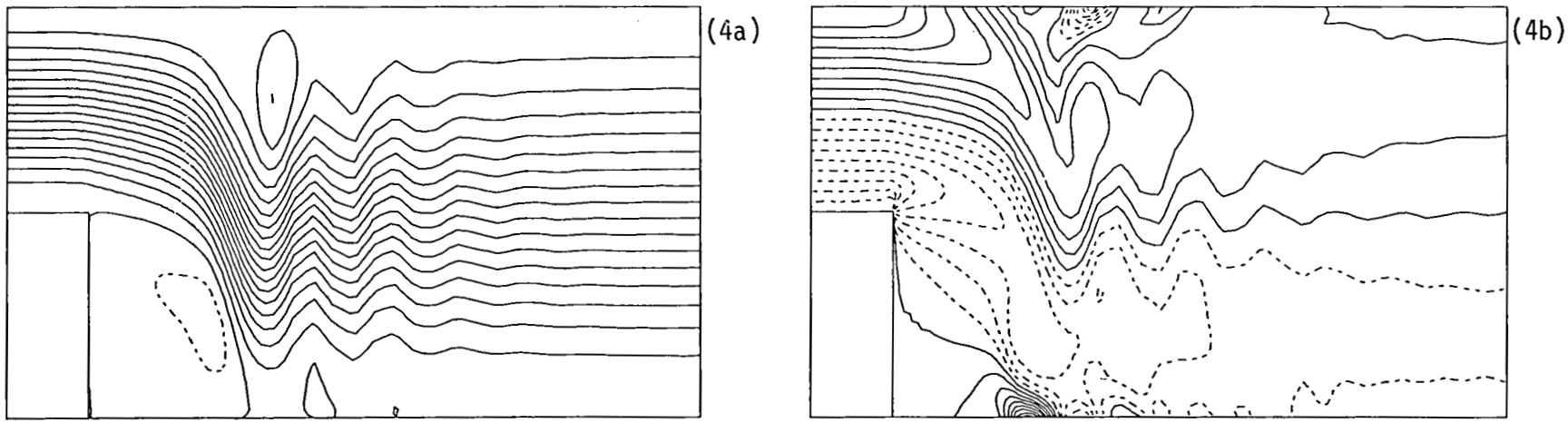

Figure 4: Channel flow with rearward facing step at Re = 500: (4a) Stream function contours (contour levels 0.0 to 0.75); (4b) Vorticity contours (contour levels -3.60 to 3.60).

1. Report No. NASA CR-172353 ICASE Report No. 84-15	2. Government Accession No.	3. Recipient's Catalog No.
4. Title and Subtitle A Numerical Study of the Two- and Three-Dimensional Unsteady Navier-Stokes Equations in Velocity-Vorticity Variables Using Compact Difference Schemes		5. Report Date May 1984 6. Performing Organization Code
7. Author(s) Thomas B. Gatski and Chester E. Grosch		8. Performing Organization Report No. 84-15 10. Work Unit No.
9. Performing Organization Name and Address Institute for Computer Applications in Science and Engineering Mail Stop 132C, NASA Langley Reserach Center Hampton, VA 23665		11. Contract or Grant No. NAS1-17070 13. Type of Report and Period Covered contractor report
12. Sponsoring Agency Name and Address National Aeronautics and Space Administration Washington, D.C. 20546		14. Sponsoring Agency Code 505-31-83-01

15. Supplementary Notes

Langley Technical Monitor: Robert H. Tolson
Final Report

16. Abstract

A compact finite-difference approximation to the unsteady Navier-Stokes equations in velocity-vorticity variables is used to numerically simulate a number of flows. These include two-dimensional laminar flow of a vortex evolving over a flat plate with an embedded cavity, the unsteady flow over an elliptic cylinder, and aspects of the transient dynamics of the flow over a rearward facing step. The methodology required to extend the two-dimensional formulation to three-dimensions is presented.

17. Key Words (Suggested by Author(s))	18. Distribution Statement
compact differences unsteady flows	34 Fluid Mechanics and Heat Transfer 64 Numerical Analysis Unclassified-Unlimited

19. Security Classif. (of this report)	20. Security Classif. (of this page)	21. No. of Pages	22. Price
Unclassified	Unclassified	20	A02

For sale by the National Technical Information Service, Springfield, Virginia 22161 NASA-Langley, 1984